ANCHORAGE BEHAVIOR OF 90-DEGREE HOOKED BEAM BARS IN REINFORCED CONCRETE KNEE JOINTS

Osamu JOH[1] And Yasuaki GOTO[2]

SUMMARY

In our previous paper, we divided the anchorage failure of 90-degree hooked bars in exterior beam-column joints in a middle story in a building into three modes: side split failure; local compression failure; and raking-out failure. The raking-out failure is raked out toward the beam side of the column due to the presence of many beam bars and/or to short development length within the joint. The purpose of this paper was to clarify the anchorage performances mainly on the raking-out failure mode of beam top-bars with 90-degree hooks arranged in an exterior beam-column joint in the roof story of a building. Thirty eight specimens of knee joints with various arrangements of L-shaped beam bar anchorage and various material properties, were subjected to pull-out loading on the beam top-bars. From the experimental results, we were able to conclude that: (1) the anchorage mechanism depends on stress transmission from the tail portion of the beam bar hooks to the adjacent column bars in a joint and that the anchorage mechanism in a knee joint was quite different from that in a exterior beam-column joint in a middle story; (2) the main factors in influencing anchorage strength are tail length, horizontal distance between tail bars and column outside-bars and between tail bars and the beam end, lateral reinforcement ratio and its strength within the joint, and concrete strength, and (3) accurate estimation of anchorage strength subjected to negative moment can be obtained by taking into account the influence of the above mentioned factors.

INTRODUCTION

Beam bars of reinforced concrete structures are usually anchored into exterior beam-column joints with a 90-degree hook. Investigations on anchorage behavior of 90-degree hooked bars are less than those on straight bar anchorage. Most of structural design codes in the world require to design the hooked bar arrangement by a specification but not a calculation. However, future design method based on performance should be changed to the style like as structural designers decide the anchorage arrangement by a calculation. Therefore, the authors investigated on performances of 90-degree hooked bars anchored into exterior beam-column joints at a middle story under experimental studies as reported in the previous papers [Ref.1, 2],and they classified the anchorage failure of 90-degree hooked bars in exterior beam-column joints at a middle story into three modes: a side split failure, a local compression failure and a raking-out failure. In the codes mentioned above, minimum values of concrete cover thickness, bar bending radius and location of bend in a joint are specified, and are provided to avoid such three anchorage failure modes, respectively. They also proposed a formula evaluating anchorage strength of 90-degree hooked bars with raking-out failure mode in consideration with some effective factors on the strength, and clarified that a share of tail portion in the resistance of hook is little.

Consecutively, the authors examined the anchorage behavior of hooked beam top-bars in beam-column knee joints, which is at a roof story of a building, in the previous paper [Ref.3] which was reported as Part One with the same title to this paper. The experiment using sixteen different specimens derived following results: 1) anchorage mechanism of hooked beam bars in knee joints located in a roof story was quite different from that in exterior beam-column joints located in a middle story, 2) anchorage strength depended on stress transmission

[1]   Architectural Engineering, Grad. School of Engineering, Hokkaido University Email: joh@eng.hokudai.ac.jp
[2]   Architectural Engineering, Grad. School of Engineering, Hokkaido University, Kita 13 Nishi 8, Kita-ku,Sapporo 060-8628

from tail bars to column bars within the joint; not on the bond behavior along the horizontal development portion of the beam bars, 3) stress transmission increased as the tail length of beam bars increased.
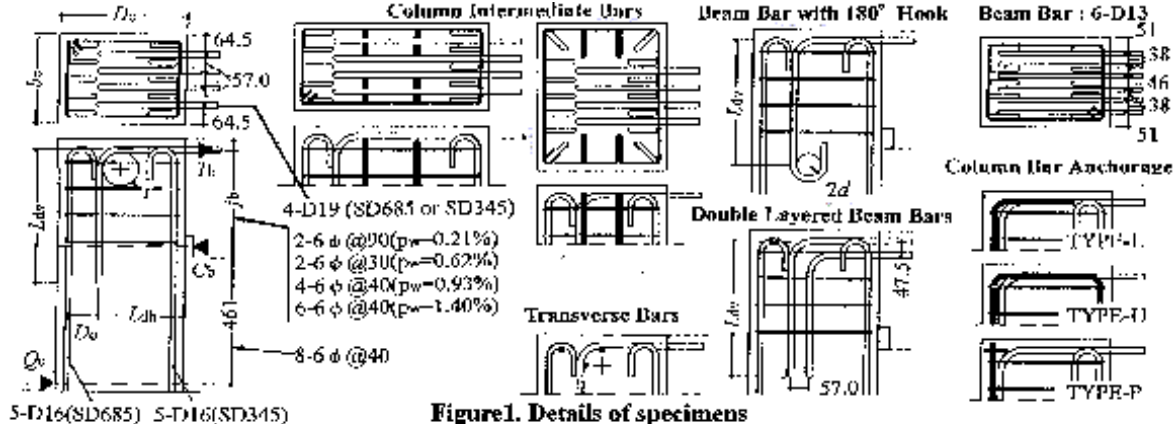
After that, the authors carried out loading tests of next sixteen specimens with wider variables in addition to the original sixteen specimens. The purpose of this paper is to propose a formula which can evaluate accurately the anchorage strength of 90-degree hooked beam-top-bars in an exterior beam-column knee joints with raking-out and side-split anchorage failure modes and be applied to more various actual arrangements of hooked bars anchored in the joint, on the basis of experimental results which were obtained from the total of thirty eight specimens subjected to a negative moment. That is, this paper is developmentally revised the previous paper[Ref.3].

EXPERIMENT

Test Specimens

Columns, about half normal size and with exterior beam-column joints at either ends, were used as specimens in this study. As shown in Figure 1, no beam concrete or compressive beam-bottom-bar were attached in order to simplify production of the specimens. Four series of specimens were tested: the TA series, with a horizontal development length L_{dh} (the distance the from beam end to the tail center) of 340mm; the TB series, with an L_{dh} of 270mm; the TC series, with an L_{dh} of 200mm; and the TBW series, with an L_{dh} of 470mm, but the TA and TB series were main. Specimens TA19-2 and TB19-2 were standard specimens from each main series and the other specimens differed from theses standard specimens in only one of test variables. The principal variable, vertical development length L_{dv} (distance from tail end to horizontal bar center), was tested at values of $8d$, $16d$, $24d$ and $32d$, where d is the nominal diameter of beam bar. These values are denoted by -1, -2,-3 and -4, respectively, being added to the specimen number. Other variables: concrete compressive strength; hoop reinforcement ratio; beam bar diameter; yield strength of beam bar; hook type of column bar; column width and depth; beam depth; number of beam layer; inside radius of beam bar hook; existence of column intermediate bars; and etc. are shown in Table 1.

The configuration as the beam bars were covered from above with $2d$, or 36 mm thick of concrete only was identical for all specimens. The values of variables in the standard specimens were $L_{dv} = 16d$, σ_B (concrete compressive strength) = 33 MPa (in design strength) and p_w (lateral reinforcement ratio within the joint) = 0.21%. The reinforcement bars of the columns were hooked 180-degrees. The beam bars were high-strength threaded deformed bar of 19 mm in diameter, four bars were arranged in a single layer, and the spacing between the center of each bar was equivalent to $3d$, or 57 mm. The inside radius of the beam bar 90-degree hook was 57 mm, or $3d$. The column specimens were 300 mm in width and 400 mm in depth. The depth of the imaginary beam was 400 mm, with a moment arm of 328 mm. The mechanical properties of the steel bars and typical concrete used in the specimens are shown in Table 2. The aggregate used was crushed stone with a maximum size of 13 mm matched to the scale of specimens. The beam bars used were a high-strength threaded and normal deformed bars of 19 mm and 13 mm in diameter, respectively.

Figure1. Details of specimens

Instrumentation and Loading

Tensile load T_b corresponding to a negative moment was applied horizontally to the beam-top-bars by a 2000kN oil-jack, as shown in Figure 1. Reaction C_b was applied at the compression zone of the imaginary beam cross section by a steel plate with a height of one-fifth beam depth, and reaction Q_c was applied to the mid-point of the out-side of the column. The four beam bars in the single layer arrangement were controlled so as to distribute the pull-out displacement equally among the bars in order to simulate actual beam bar conditions. Thus the tensile loads on each bar varied slightly. The eight beam bars in the double layer bar arrangement also were controlled under the same loading way.

Table1. Variations of specimens

Specimen	Ldh (mm)	Ldv	Variations	Specimen	Ldh (mm)	Ldv	Variations
TA19-1	340	8d	⎫	TB19-4	270	32d	(Standard)
TA19-2	340	16d	⎬ (Standard)	TB19-4RO	270	32d	bc=500mm T
TA19-3	340	24d	⎭	TB19-2P2	270	16d	pw=0.62%
TA19-2CL	340	16d	fc=20MPa	TB19-2P3	270	16d	pw=0.93%
TA19-2CH	340	16d	fc=45MPa	TB19-2P4	270	16d	pw=1.40%
TA19-2W	340	16d	Dc=470mm	TB19-3J2	270	24d-100mm ib=228mm T	
TA19-1A	340	8d	P	TB19-3J3	270	24d+100mm ib=428mm T	
TA19-2A	340	16d	P	TB19-2W	270	16d	Dc=470mm
TA19-3A	340	24d	P	TB19L-2	270	16d	Beam Bar : SD345
TA19-3RO	340	24d	bc=500mm P T	TB19R-2	270	16d	r=5d
TA19-2S	340	16d	L	TB19D-2	270	16d	bc=500mm D.T
TA19-2IS	340	16d	II	TB19D-3	270	24d	bc=500mm D.T
TA19-2AP2	340	16d	pw=0.62% P	TB19H-4	270	32d-10d bc=500mm H.T	
TA19-4TR	340	32d	T	TB19-2M	270	16d	bc=500mm M T
TA13-1	340	8d	Beam Bar : 6-D13	TB19-5TR	270	40d	T
TA13-2	340	16d	Beam Bar : 6-D13	TC19-2	270	16d	(Standard)
TB19-1	270	8d	⎫	TC19-2P2	200	16d	pw=0.62%
TB19-2	270	16d	⎬ (Standard)	TBW19-2	470	16d	Dc=600mm
TB19-3	270	24d	⎭	TBW19-2M	470	16d	Dc=600mm M

*d is Diameter of Beam Bar

*Standard :
fc=30MPa, pw=0.21%,
Dc=400mm, hc=300mm
r=3d, ib=328mm
Column Bar 180°Hook
Beam Bar : 4-D19/SD685

*P.L.U: TYPE of Column Bar.
*T : Transvers Bars
*H : Beam Bar with 180°Hook
*M : Column Intermediate Bars.
*D : Double Layered Beam Bars

Table2. Measured properties

CONCRETE (example)	E^{1/3} (GPa)	E^{2/3} (GPa)	εmax (μ)
σB=26.3MPa	21.8	18.8	2760
σB=34.2MPa	25.5	21.4	2830
σB=44.7MPa	26.8	23.8	2920

STEEL	σy (MPa)	εy (μ)	σmax (MPa)	Es (GPa)
D19(SD685)	667	3560	892	187
D19(SD345)	386	2140	582	192
D16(SD685)	795	4250	911	187
D16(SD345)	384	2380	555	161
D13(SD685)	728	3590	927	199
6φ(SR345)	369	1720	486	215

EXPERIMENTAL RESULTS AND DISCUSSION

Behavior of Cracks and Failure

Figure 2 is a schema showing a typical crack pattern that appeared on the side of specimens at the final loading stage and showing the mark of each crack. The cracking process occurred as follows: (1) a flexural crack F appeared at the bottom of the joint in the tensile region but did not open widely; (2) the crack SF appeared in the end of the column near the mid-point of the horizontal straight portion of the bar in the joint and extended to the compression corner reducing the stiffness of the joint; (3) the crack S appeared at the bend of the bar, extended to the compression corner severely reducing the stiffness of the joint and led usually specimens of the TA series to the ultimate stage; (4) the crack V started along the bar bend, extended along the tail of bar and led usually specimens of the TB series to the ultimate stage; and (5) the crack SH branched out from the crack V and extended towards the compression zone.

Failure Modes

Figure 3 is a schema showing typical failure modes obtained from this test. Crack patterns of some specimens taken after the loading test are shown in Figure 4. The failure modes were divided into four classes according to guidelines described in our previous paper.

(1) Raking-out anchorage failure (AR). A concrete block, approximating the inside dimensions of the hooked bar in size, is raked out toward the beam side of the column while rotating on the compression corner. The ultimate stage of this failure mode was led by opening crack S for TA series and crack V for TB series specimens and was due to bond failure of the tail of the bars.

(2) Side-split anchorage failure (AS). The concrete covering the bent portion of the beam or column bars in a joint peels away leaving a dish-shaped depressions individually on both sides of the joint. This type of failure is due to split stress around the inside of the bend portion of the bars. Many TA series specimens failed in side split of concrete beside the column (not beam) bar hooks, simultaneously with raking-out failure.

(3) Fracture of the column bar hook (FR). The bend portions of the column bars are broken by bending reversal resulting from an increase in deformation.

(4) Shear failure of joint (JS). The concrete around the compression corner in a joint is crushed after the development of a crack S. No specimen in this study demonstrated evidently this type of failure.
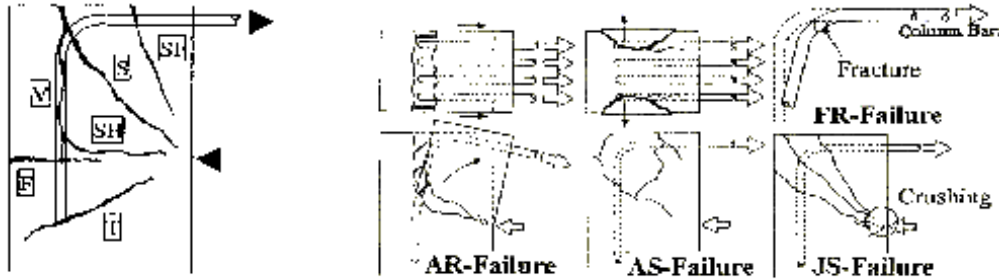

Figure2. Typical cracks

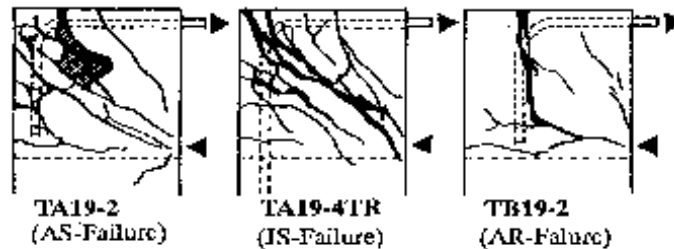**Figure3. Failure modes in beam-column joint**

Figure4. Examples of crack patterns after loading test

Load vs. Displacement Relationship

Some examples of Load vs. displacement curves, selecting out of TB series, are shown in Figure 5, and relationships between the type of cracks and the stiffness deterioration appearing on the curves are schematically shown in Figure 6. The displacement was measured as relative displacement between a point on beam bars on the column face and the mid point of the column depth. As it is clear from Figure 5 and the curves (b) in Figure 6, the stiffness of the joints with large L_{dv} value declined gradually due to an S-crack and/or V-crack and load resistance after maximum load also deteriorated gradually, regardless of their failure modes. However, the joints with low L_{dv} values, for example of TB19-1 and TB19-2, led to a severe deterioration in load resistance soon after the onset of a decrease in the stiffness of the joints as indicated by the curves (a) in Figure 6, and such joints failed in the raking-out. In the case of large L_{dh} as shown Figure 6(ii), the first stiffness declination appeared due to an SF-crack before appearing due to the S-crack and/or V-crack. The experimental load resistances at the first stiffness declination $_{exp}T_d$ and the ultimate stage $_{exp}T_u$ are inserted in Table 3. The table shows that the values $_{exp}T_d$ of specimens indicated the curves (a) were identical with the values of $_{exp}T_u$. The numbers of specimens failed in AR, AS, JS and FR mode are twenty six, eight, three and one, respectively.
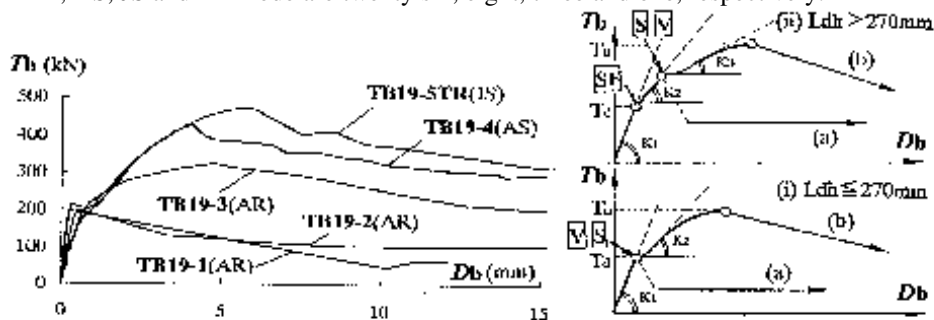

Figure5. T_b vs. D_b relation-curves

Figure6. Typical curves of T_b vs. D_b

Table 3. Observed and calculated anchorage strengths

Specimen	Experimental Results					Calculated Results						$\frac{_{exp}T_u}{_{cal}T_u}$
	σ_B (MPa)	$_{exp}T_d$ (kN)	$_{exp}T_u$ (kN)	$_{exp}T_u'$ (kN)	Failure Mode	$_{AR-a}T_u$ (kN)	$_{AR-b}T_u$ (kN)	$_{AR}T_u$ (kN)	$_{AS}T_u$ (kN)	$_{JS}T_u$ (kN)	$_{cal}T_u$ (kN)	
TA19-1	34.2	177	299	280	AR	237	80	237	390	541	237	1.26
TA19-2	34.2	195	403	377	AS	-	-	255	390	541	390	1.03
TA19-3	35.7	229	516	473	AS	-	-	572	396	557	396	1.30
TA19-2CL	26.3	218	431	460	AS	-	-	240	351	450	351	1.23
TA19-2CH	44.7	196	490	401	AS	-	-	271	434	692	434	1.13
TA19-2W	33.3	196	247	234	AR	234	108	234	385	531	234	1.06
TA19-1A	33.8	197	236	222	AR	236	80	236	388	537	236	1.00
TA19-2A	38.5	233	333	294	AR	252	262	262	409	588	262	1.27
TA19-3A	33.8	212	484	456	AS	-	-	388	388	537	388	1.25
TA19-3RO	33.6	274	566	535	AR	387	557	557	732	818	557	1.02
TA19-2S	38.5	290	498	440	FR	-	-	262	409	588	409	1.22
TA19-2JS	32.5	256	487	468	AS	-	-	252	382	522	382	1.28
TA19-2AP2	32.5	278	370	364	AR	244	447	447	382	522	447	0.85
TA19-4TR	36.2	278	648	590	JS	-	-	912	399	563	563	1.15
TA13-1	35.8	157	266	244	AR	243	41	243	397	559	243	1.10
TA13-2	35.8	195	364	333	AR	243	138	243	397	559	243	1.50
TB19-1	39.1	196	196	172	AR	201	26	201	334	472	201	0.97
TB19-2	39.1	199	199	174	AR	201	92	201	334	472	201	0.99
TB19-3	35.7	215	325	298	AR	203	319	319	322	443	319	1.02
TB19-4	34.9	210	429	398	AS	-	-	566	319	436	319	1.34
TB19-4RO	33.6	-	598	565	JS	-	-	554	596	650	650	0.93
TB19-2P2	38.1	206	284	252	AR	210	228	228	331	463	228	1.24
TB19-2P3	23.0	177	264	302	AR	163	277	277	270	325	277	0.95
TB19-2P4	33.4	194	388	368	AR	196	393	393	314	423	393	0.97
TB19-3T2	33.3	195	410	398	AR	196	369	369	362	422	369	1.13
TB19-3T3	33.3	189	338	321	AR	196	288	288	288	422	288	1.18
TB19-2W	33.3	187	197	187	AR	186	66	186	313	422	186	1.06
TB19L-2	36.9	207	207	187	AR	196	92	196	327	453	196	1.06
TB19R-2	23.0	167	167	191	AR	154	88	154	220	325	154	1.08
TB19D-2	34.5	334	315	294	AR	290	91	290	602	662	290	1.09
TB19D-3	34.2	353	431	404	AR	310	312	312	600	658	312	1.38
TB19H-4	34.2	267	374	350	AR	289	251	289	600	658	289	1.30
TB19-2M	35.2	275	275	254	AR	293	91	293	607	671	293	0.94
TB19-5TR	34.7	196	476	443	JS	-	-	814	319	434	434	1.10
TC19-2	34.9	158	158	146	AR	141	56	141	254	323	141	1.12
TC19-2P2	33.4	137	181	172	AR	145	150	150	249	313	150	1.21
TRW19-2	32.1	198	341	330	AR	318	130	318	531	715	318	1.07
TRW19-2M	32.1	216	431	417	AS	-	-	318	531	715	531	0.81

Influence of Variables on Anchorage Strength

In order to compensate for effect of dispersion of actual concrete strength in all specimens on the anchorage strength, normalized anchorage strength $_{exp}T_u'$, calculated by the equation $(= T_u\sqrt{30/\sigma_B})$ which converted into design concrete strength of 30 MPa, was used. The relationship between $_{exp}T_u'$ and the horizontal development length L_{dh} is shown in Figure 7. The $_{exp}T_u'$ increased linearly with increases in L_{dh} in the region of a lateral distance between the tails of the beam bars and the column-outside-bars, D_o, equal to and larger than 95 mm as shown with the round marks in the figure. However, the $_{exp}T_u'$ for TA19-2A increased with decreases in D_o although L_{dh} had the same value. The $_{exp}T_u'$ for TA19-2 increased much more as the column anchorage of 180-degree hooks was used even though the D_o values were equal, because the tails of the column hooks crossed the beam bars and prevented premature cracks between the column bars and the beam tail bars.

The relationship between $_{exp}T_u'$ and L_{dv} is shown in Figure 8. The $_{exp}T_u'$ increased with increases in L_{dv} in TA series specimens and the increase rate became large remarkably in the region in which the vertical development length L_{dv} was larger than a moment arm of beam j_b (= 328 mm). This means that tensile stress applied to the tails of the beam bars was transmitted to the tensile column bars in a joint according to the lapped bar-joint stress transmission mechanism. Stress transmission in TA19-2L, with 90-degree column bar hooks, was higher than that in TA19-2, which had 180-degree hooks, and that in TA19-2A, without hooked column bars, was lower than that in TA19-2. The $_{exp}T_u'$ in the TA series specimens was found to be larger than that in the TB series specimens. The reasons for these larger $_{exp}T_u'$ values are thought to be: 1) tail stress T_t in the TA specimens was larger because of the short lateral distance D_o, and 2) the resistant moment on the reaction point expressed by L_{dh} x T_t was larger in the TA specimens than in the TB specimens because of their longer L_{dh}. Test results also indicated that the increase rate in TB series specimens was less than that in TA series, especially $_{exp}T_u'$ in the TB specimens with an L_{dv} less than the moment arm of the beam (j_b = 328mm) was low because the column hooks were situated further from the beam bars so that a premature crack along the tail of the hooked bar (V-crack in Figure 2) prevented the transmission of the tail stress to the column bars. The $_{exp}T_u'$ value for TB19-3, which had an L_{dv} longer than the moment arm of the beam, was large because the V-crack along the tail could not expand into the horizontally compressive zone in the column.
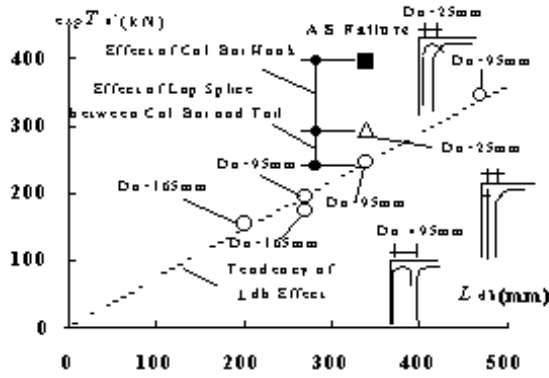
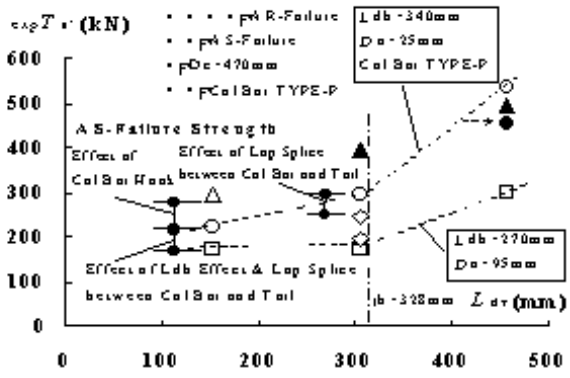Figure7. Relationship of $_{exp}T_u'$ and L_{dh} Figure8. Relationship of $_{exp}T_u'$ and L_{dv}

Evaluation of Anchorage Strength with Raking-out Failure

The raking-out failure can be classified to two cases. In one case, the maximum resistance appeared at occuring the S- and/or V-crack as shown the curve-(a) in Figure 5, and it is named a shear crack type. In the other case, the maximum resistance was reached in the middle of bond failure of beam bar tails after those cracks as shown the curve-(b) in the figure, and it is named a bond failure type.

Raking-out failure in shear crack type was caused by S-crack mainly even though V-crack appeared, therefore the ultimate strength can be evaluated by using a calculation of diagonal shear crack strength:

$$_{AR-s}T_u = 0.47 \cdot L_{dh} \cdot b_j \cdot \sqrt{\sigma_B} \tag{1}$$

where b_j is the effective joint width according to the reference 4.

In the case of raking-out failure in bond failure type, a model of stress transmission in a joint after occurring vertical-cracks along the beam bar tails is derived from the tie-strut model which is based on an equilibrium of tensile forces by steel ties and compressive forces by concrete struts as shown in Figure 9. Each force showing in the figure was calculated on the following mechanical assumptions: (1) the ultimate resistance appears at bond failure of the tails except the length of V-crack along the tails, x_{cr}, (2) lateral force of hoops in a joint T_w is equal to the total yield force of the hoops crossing the V-crack, (3) a working point of each force is on the center of effective area in which the stress by each force distributes.
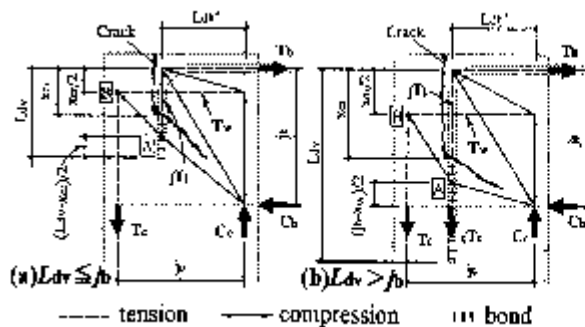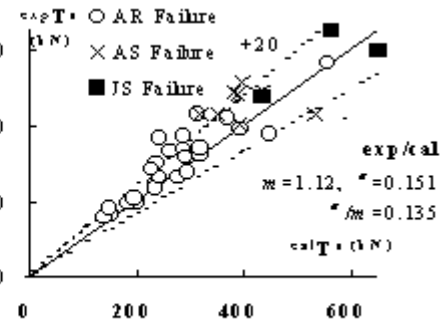

Figure9. Tie-Strut model   Figure10. Comparison with proposed equations

The $_jT_t$ and $_cT_t$ are the forces acting within the V-crack zone and its remaining zone, respectively. These forces are expressed by the following equations for two cases: L_{dv} is less than j_b and is larger than j_b, according to the behavior mentioned in the section 3.4.

$$_jT_t = {}_j\tau_u \cdot n \cdot \phi \cdot (L_{dv} - x_{cr}) \qquad (L_{dv} \leq j_b) \tag{2a}$$

$$\left. \begin{array}{l} _jT_t - {}_cT_t = {}_j\tau_u \cdot n \cdot \phi \cdot (j_b - x_{cr}) \\ _cT_t = {}_c\tau_u \cdot n \cdot \phi \cdot (L_{dv} - x_{cr}) \end{array} \right\} \qquad (L_{dv} > j_b) \tag{2b}$$

where n is the number of beam bars, ϕ is the perimeter of beam bars, x_{cr} is the length of V-crack, $_j\tau_u$ and $_c\tau_u$ are the bond strength of beam bars in the joint and in the column, respectively.

These bond strength are obtained by the following equation:

$$_j\tau_u = {}_c\tau_u = 0.94 \cdot \sigma_B^{2/3}.$$ (3)

The multiplier in this evaluation, which was provided in the guidelines of AIJ[Ref.4], was modified on our test results. In this paper, both the strength were considered to be the same value for convenience although they might be different originally. The lateral force of hoops in the joint T_w can be derived from the assumption-(2) as follows:

$$T_w = b_c \cdot p_w \cdot \sigma_{wy} \cdot x_{cr},$$ (4)

where p_w is the ratio of hoops in the joint and σ_{wy} is the tensile strength of the hoops. The x_{cr} is derived from the equilibrium of stresses at the point A which is the center of the remaining length subtracted the V-crack length x_{cr} from the joint height, as shown in Figure 9.

$$x_{cr} = (j_b - L_{dv} \cdot j_c / 2D_o - \lambda) + \sqrt{(j_b - L_{dv} \cdot j_c / 2D_o - \lambda)^2 + 2L_{dv} \cdot \lambda}, \qquad (L_{dv} \le j_b)$$ (5)

where $\lambda = ({}_j\tau_u \cdot n \cdot \phi / b_c \cdot p_w \cdot \sigma_{wy}) \cdot L_{dh}'$ and $L_{dh'}$ is the lateral distance between the beam bar tails and the column compressive bars. However L_{dv} in this equation should be changed to j_b when L_{dv} is longer than j_b. From the equilibrium of stresses at the point B which the resultant force of the hoops T_w and of the column tensile bars T_c cross at, as shown in Figure 9, T_c is derived as follows:

$$T_c = (L_{dv} / 2D_o) \cdot T_w. \qquad (L_{dv} \le j_b)$$ (6)

However L_{dv} in this equation should be changed to j_b when L_{dv} is longer than j_b.
And also from the equilibrium of whole stresses surrounding the joint, the following relations are derived:

$$T_b \cdot j_b = T_c \cdot j_c, \qquad (L_{dv} \le j_b)$$ (7a)

$$T_b \cdot j_b = T_c \cdot j_c + {}_cT_t \cdot L_{dh}'. \qquad (L_{dv} > j_b)$$ (7b)

This value T_b corresponds to the anchorage strength with raking-out failure in the bond failure type $_{AR\text{-}b}T_u$. Finally the anchorage strength with raking-out failure $_{AR}T_u$ is obtained as the largest value between the strength of $_{AR\text{-}s}T_u$ and $_{AR\text{-}b}T_u$ calculated by Equations-(1) and -(7), respectively.

Both strengths for the whole specimens are shown in Table 3 and the relation between the calculated and experimental results for twenty six specimens failed in raking-out mode is shown by plotting with round marks in Figure 10. The average of λ, which is the ratio of experimental maximum strength $_{exp}T_u$ to calculated ultimate strength $_{cal\text{-}AR}T_u$ for the twenty six specimens was 1.10 and the standard deviation was 0.15. One of the reasons why the value of λ was larger than 1.0 is that the effect of column bar hooks on strengthening the anchorage strength for A-series specimens with beam bar tails L_{dv} shorter than j_b was not considered.

Evaluation of Anchorage Strength with Side-split Failure

The evaluation formula of anchorage strength with side-sprit failure for exterior beam-column joints located in a middle story $_{AS}T_u$ is provided in the guideline mentioned before [Ref.4] as follows:

$$_{AS}T_u = f_u \cdot A_b$$ (8a)

$$f_u = 210 \cdot k_c \cdot k_j \cdot k_d \cdot k_s \cdot \sigma_B^{0.4},$$ (8b)

where A_b is the total cross-sectional area of beam bars, f_u is the anchorage strength per an unit cross-sectional area of bars, k_c, k_j, k_d, and k_s are the effective factors of the concrete cover thickness, the configuration of the joint, the development length and the amount of hoops arranged on the hooks, respectively. The relationship between the experimental maximum resistance $_{exp\text{-}AS}T_u$ and the calculated strength $_{cal\text{-}AS}T_u$ is shown in Figure 10. The deviation of $_{cal}T_u$ from $_{exp}T_u$ was very small, but the calculated values were overestimated to the experimental results, because the confinement of the cover-concrete to the hooks become low owing no column above the joint. Therefore we proposed the following equation using the modification factor $_{AS}\kappa$ of 0.8 for beam-column joints in the roof story subjected negative moment.

$$f_u = {}_{AS}\kappa \cdot 210 \cdot k_c \cdot k_j \cdot k_d \cdot k_s \cdot \sigma_B^{0.4}.$$ (8c)

Evaluation of Shear Strength of Knee Joints

The evaluation formula of shear strength of joints $_{JS}T_u$ provided in the guidelines is used in this discussion.

$$_{JS}T_u = V_{ju} = \kappa \cdot \phi \cdot F_j \cdot b_j \cdot D_j, \tag{9}$$

where κ is the configuration factor of joints, ϕ is 0.85 for no transverse beam, F_j is the effective concrete strength for shear failure ($=0.8\,\sigma_B^{0.7}$). b_j is the effective width of beams, and D_j is L_{dh} for exterior beam-column joints. The configuration factor of joints κ is 0.7 and 0.4 for T-shaped and L-shaped (knee) joints, respectively. However the calculated strength of the three specimens failed in shear were overestimated with about 1.7 times as large as the experimental results when κ of 0.4 was used, but showed the good approximate values of 0.97 times when κ of 0.7 was used. This means the shear strength of knee joints subjected to negative moment can be evaluated as the same value of joints in the middle story. The κ factor of 0.4 may be applied to the knee joints subjected positive moment.

Comparison between the experimental and calculated strengths in three different failure modes

Table 3 shows the maximum resistance of the whole specimens $_{exp}T_u$ and the calculated ultimate strength $_{cal}T_u$ which was obtained by using the equation for failure mode resulted in each specimen. The relation between the $_{cal}T_u$ expressed by bold numbers in the table and $_{exp}T_u$ are shown in Figure 10. The average ratio of the experimental to calculated strengths for the whole specimens was 1.12 and the standard deviation was 0.15. Therefore most beam-column knee joints can be divided to fail in three failure modes when the evaluations are used with a decreasing factor of 0.8.

CONCLUSIONS

We examined the anchorage between of beam-column knee joints using columns with 90-degree hooked beam top bars subjected pull-out loading. The test variables of the specimens were horizontal and vertical development lengths, lateral reinforcement ratio and its strength in the joint, concrete strength, hook type of column bars, etc. The conclusions obtained from the experimental results are as follow:

1)Relationship of anchorage mechanisms of hooked beam top bars subjected pull-out loading in between knee joints located in a top story and beam-column joints located in a middle story was quite difference when the joint failed in raking-out mode, but was relatively similar when the joint failed in side-split mode. The relationship of shear mechanisms of them in between both joints was quite similar.

2)Anchorage strength with the raking-out failure mode depended on stress transmission from beam tail bars to column tensile bars, therefore the evaluation of the strength should be considered with a lateral distance between both bars and the tail length of beam bars mainly.

3)Evaluation for anchorage strength with the side-split failure mode needed to be used with a modification factor of 0.8 against the previous equation applied to joints in a middle story, because the confinement of cover concrete to the hooks was low by the luck of upper column.

4)Shear strength of the joints might be used by using the previous equation for the shear failure applied to joints in a middle story mode without modification.

5)Experimental results based on our test of thirty eight specimens confirmed the accuracy of our newly proposed evaluation for raking-out anchorage failure, our modified equation for side-split anchorage failure and the previous equation for shear failure.

REFERENCES

1. Joh,O., Goto,Y. & Shibata,T.(1995), "Anchorage of Beam Bars with 90-Degree Bend in Reinforced Concrete Beam-Column Joints", *Proc. of the Tom Paulay Symposium "Resent Development Lateral Force Transfer in Building," American Concrete Institute*, SP-157, pp.97-116

2. Joh,O. & Shibata,T.(1996), "Anchorage Behavior of 90-Degree Hooked Beam Bars in Reinforced Concrete Beam-Column Joints", *Proc. of the 11th World Conference on Earthquake Engineering,* Acapulco, CD-ROM-3

3. Joh,O. & Goto,Y.(1999), "Anchorage Behavior of 90-Degree Hooked Beam Bars in Reinforced Concrete Knee Joints", *Proc. of ERES 99*, pp.33-42

4. Architectural Institute of Japan(1997), *Design Guideline for Earthquake Resistant Reinforced Concrete Buildings Based on Inelastic Displacement Concept (Draft)*